Dynamic Modeling of Surface-Mounted Permanent Magnet Motors Considering Saturation

Zhaokai Li
College of Electrical Engineering
Zhejiang University
Hangzhou, China
lzk_zju@zju.edu.cn

Yuzheng Chen
Power Electronics, Machines, and
Control Group
University of Nottingham
Nottingham, United Kingdom
yuzheng.chen@nottingham.ac.uk

Xiaoyan Huang
Zhejiang Provincial Key Laboratory of
Electrical Machine Systems
Zhejiang University
Hangzhou, China
xiaoyanhuang@zju.edu.cn,

Xinru Li, Wucheng Ying, Boyang Shen
Department of Engineering
University of Cambridge
Cambridge, United Kingdom
xl418@cam.ac.uk, wy256@cam.ac.uk,
bs506@cam.ac.uk

Lijian Wu, Youtong Fang
College of Electrical Engineering
Zhejiang University
Hangzhou, China
youtong@zju.edu.cn, ljw@zju.edu.cn

Teng Long
Department of Engineering
University of Cambridge
Cambridge, United Kingdom
tl322@cam.ac.uk

Abstract—**This paper developed a dynamic hybrid field model (DHFM) for surface-mounted permanent magnet (SPM) motors coupled with external drive circuit considering motor saturation. In the proposed model, the iron saturation of SPM motor is equivalently replaced by the saturation current in the slot opening and therefore the analytical solution of the air-gap field is determined. Based on the air-gap field, the total flux linkage and electromagnetic torque is calculated. The instantaneous inductance is also derived from DHFM using frozen permeability method. The instantaneous back-EMF is determined by the flux linkage produced by PM separating from the total flux linkage. Hence, according to the circuit model and mechanical model, the winding current at next step can be obtained. The proposed model is more efficient in terms of computation and its accuracy is validated by FEM results.**

Keywords—hybrid field model, motor control, iron saturation

I. INTRODUCTION

Permanent magnet (PM) motor has drawn worldwide attention due to its high power density and compact structure. The transient analysis of PM motor is usually carried out using FEM software, which is accurate but time-consuming[1]. Fazil *et al.* proposed a nonlinear dynamic model based on the lookup table. The table data is calculated from static finite-element results, which accounts for the iron nonlinearity of the motor [2]. Xuan *et al.* developed the winding function model for fractional slot PM motors and calculated the three-phase short circuit current [3]. The main difficulty of coupling the motor model with external circuit is to account for the iron saturation of the motors in the drive circuit. Hence, this paper introduced a dynamic hybrid field model which gives the analytical solution for nonlinear SPM motors. Based on the circuit model, the SPM motor is accordingly represented by the winding resistance, nonlinear inductance, and instantaneous back-EMF in voltage source inverter. For the mechanical model, the rotor speed can be described, which is used to calculated the instantaneous back-EMF. Therefore, the transient analysis of SPM motor is carried out to show its dynamic performance. The proposed model significantly reduces the computational time and shows high accuracy.

II. NONLINEAR DYNAMIC MODELLING

The proposed dynamic hybrid field model is divided into three parts: the accurate motor model based on static hybrid field model [4]-[5], the circuit model, and the mechanical model. Since the SPM motor can be generalized by the static hybrid field model, the nonlinear inductance and instantaneous back-EMF can be calculated. Based on the mechanical model, the rotational speed of motor is obtained and therefore the back-EMF can be calculated considering saturation. In the circuit model, the SPM motor is equivalent to the nonlinear inductance in series with the voltage source (back-EMF) and winding resistance. Hence, the winding current at the next step will be determined according to the voltage balance equation.

A. Accurate Motor Model Based on Hybrid Field Model

For the accurate motor model, the iron saturation of SPM motor is represented by the equivalent current. In this way, the magnetic field in the air-gap can be analytically obtained from the supposition of the magnetic field generated by PM, winding current and equivalent current representing iron saturation.

$$B_{air\_r} = B_{PM\_r} + B_{winding\_r} + B_{sat\_r} \tag{1}$$

$$B_{air\_\theta} = B_{PM\_\theta} + B_{winding\_\theta} + B_{sat\_\theta} \tag{2}$$

where B_{PM_r} and B_{PM_α}, B_{wr} and $B_{w\alpha}$ B_{sat_r} and B_{sat_α} are the radial and tangential air-gap flux density produced by the PMs, winding current, and the equivalent saturation current, respectively. Hence, the analytical air-gap field produced by the PMs is derived as

$$B_{mr}(\theta, r) = \sum_{n=1,3,5,\cdots}^{\infty} K_B(n) f_{Br}(r) \cos(np\theta) \tag{3}$$

$$B_{m\alpha}(\theta, r) = \sum_{n=1,3,5,\cdots}^{\infty} K_B(n) f_{B\theta}(r) \sin(np\theta) \tag{4}$$

where $f_{B\theta}(r), f_{Br}(r)$, and $K_B(n)$ can be found in [4].

The general solution of analytical the air-gap field produced by the current including the winding current, the saturation current and the is calculated as [5]

$$
\begin{aligned}
B_{cr} = \frac{\mu_0}{\pi} \sum_{k=1}^{Q_s} \sum_{v} \Bigg\{ & \frac{i_{ssk} + i_{wk}}{v} K_{sov}(b_0) F_v(r) \sin\left[v\left(\alpha - \frac{2k\pi}{Q_s} \right) \right] + \\
& \frac{i_{tlk}}{v} K_{sov}\left(\frac{t_0}{2}\right) F_v(r) \sin\left[v\left(\alpha - \frac{(2k-1)\pi}{Q_s} + \frac{t_0}{4R_s} \right) \right] + \\
& \frac{i_{trk}}{v} K_{sov}\left(\frac{t_0}{2}\right) F_v(r) \sin\left[v\left(\alpha - \frac{(2k-1)\pi}{Q_s} - \frac{t_0}{4R_s} \right) \right] \Bigg\}
\end{aligned}
\tag{5}
$$

$$B_{c\alpha} = \frac{\mu_0}{\pi} \sum_{k=1}^{Q_s} \sum_v \left\{ \frac{i_{ssk} + i_{wk}}{v} K_{sov}(b_0) G_v(r) \cos\left[v\left(\alpha - \frac{2k\pi}{Q_s}\right)\right] + \right.$$
$$\frac{i_{tlk}}{v} K_{sov}\left(\frac{t_0}{2}\right) G_v(r) \cos\left[v\left(\alpha - \frac{(2k-1)\pi}{Q_s} + \frac{t_0}{4R_s}\right)\right] +$$
$$\left. \frac{i_{trk}}{v} K_{sov}\left(\frac{t_0}{2}\right) G_v(r) \cos\left[v\left(\alpha - \frac{(2k-1)\pi}{Q_s} + \frac{t_0}{4R_s}\right)\right]\right\}$$
$$(6)$$

where K_{sov}, G_v, and F_v are

$$K_{sov}(\beta) = \frac{\sin(v\beta/2R_s)}{v\beta/2R_s} \tag{7}$$

$$G_v(r) = \frac{v}{r}\left(\frac{r}{R_s}\right)^v \frac{1-(R_r/r)^{2v}}{1-(R_r/R_s)^{2v}} \tag{8}$$

$$F_v(r) = \frac{v}{r}\left(\frac{r}{R_s}\right)^v \frac{1+(R_r/r)^{2v}}{1-(R_r/R_s)^{2v}} \tag{9}$$

It is noted that the detail about the slotting effect represented by the complex permeance function can be found in [4]-[5]. For accurate calculate of the equivalent saturation current, the field distribution in the stator iron should be determined first from the magnetic equivalent circuit (MEC) in Fig. 1. Since the total current considering saturation is proportional to the magnetic potential drop along the stator bore for the proposed model, the air-gap flux linkage can be modelled as the voltage controlled current source, as shown in Fig. 1. The iterative calculation is required to solve the coupling of the analytical air-gap field and the magnetic equivalent current. Fig. 1 also gives the details of the hybrid field model for SPM motor.
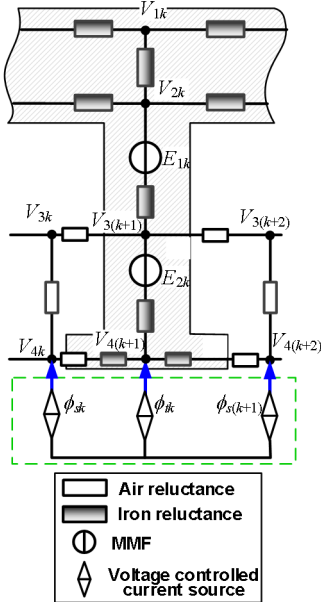

Fig. 1. The magnetic equivalent circuit for one-slot and air-gap region in the static hybrid field model.

According to Kirchhoff's laws, the mathematic formula of Fig. 1 can be expressed as

$$f(\mathbf{V}) = \mathbf{A}\left[\mathbf{\Lambda}\mathbf{A}^{\mathbf{T}} - \mathbf{R}_{ss}\mathbf{C}_{ss}\right]\mathbf{V} - \mathbf{A}\mathbf{\Lambda}\mathbf{E} - \mathbf{A}\mathbf{\Phi}_{\mathbf{PM}} = 0 \quad (10)$$

where $\mathbf{V}$, $\mathbf{E}$, $\mathbf{\Lambda}$, and $\mathbf{A}$ means the matrixes of the node magnetic potential, branch MMF, branch permeance, and incidence, respectively. $\boldsymbol{\varphi}_{\mathbf{PM}}$ is the matrixes of the air-gap flux produced by PM neglecting saturation. $\mathbf{R}_{ss}$ is used to calculate the fluxes

flowing into the stator teeth and slots due to the total current considering saturation. $\mathbf{C}_{ss}$ connects the magnetic potential drop in the iron with the total current including equivalent saturation current and winding current. More details can be seen in [4]-[5].

The total flux linkages ψ_{ph} is derived as:

$$\psi_{ph}(t) = \sum_{i=1}^{\kappa} \left(\psi_{ti}(t) + \psi_{li}(t)\right) \tag{11}$$

where Ψ_{ti} is the main flux linkage flowing into the stator teeth and Ψ_{li} means the leakage flux calculated from MEC in the SPM motor. They are obtained from the tangential air reluctance in the slots and slot openings in the magnetic equivalent circuit of Fig. 1.

The inductance of each phase is calculated using frozen permeability method. Assuming that $\mathbf{\Lambda}$ calculated from (1) stays unchanged and $\mathbf{\Phi}_{\mathbf{PM}}$=0, the flux linkage produced by each phase current can be obtained in the static hybrid field model. Therefore, the inductance is calculated and the flux linkage produced by winding current and PM can be separated to determine the back-EMF. The saturation coefficient of back-EMF is defined as

$$c_{emf}(\theta) = \frac{\psi_{ph\_PM}(\theta)}{\psi_{PM}(\theta)} \tag{12}$$

where ψ_{ph_PM} is the separated PM flux linkage and ψ_{PM} is the flux linkage under open-circuit condition neglecting saturation. The back-EMF considering saturation is calculated by

$$E_{ph} = c_{emf}(\theta) * E_{PM} \tag{13}$$

where E_{PM} is the back-EMF of the SPM motor under open-circuit condition neglecting saturation. Besides, the electromagnetic torque of the SPM machine can be calculated as [4]

$$T_e = \frac{1}{\mu_0} l_{ef} r^2 \int_0^{2\pi} B_r B_\alpha d\alpha \tag{14}$$

where B_r and B_α are the radial and tangential flux density along the circle of the air-gap whose radius is r, and l_{ef} represents the effective length of the SPM motor

B. Circuit Model and Mechanical Model

In the circuit model, the voltage balance of each phase can be expressed as the matrix form:

$$\mathbf{V}_{abc} = \mathbf{L}_{abc} \frac{d\mathbf{I}_{abc}}{dt} + \mathbf{R}_{abc}\mathbf{I}_{abc} + \mathbf{E}_{abc} \tag{15}$$

where the $\mathbf{L}_{abc}$ is the matrix of self and mutual inductance for each phase while $\mathbf{E}_{abc}$ is the matrix of back-EMF. They are obtained from the static hybrid field model. $\mathbf{R}_{abc}$ is the phase resistance. $\mathbf{V}_{abc}$ and $\mathbf{I}_{abc}$ are the phase voltage and phase current in the circuit model.

Hence the instantaneous phase current can be obtained according to KVL. Fig. 2 shows the proposed circuit model to calculate the phase current. It is noted that the phase winding is represented by the inductance, instantaneous back-EMF calculated from the static hybrid field model, and the winding resistance.
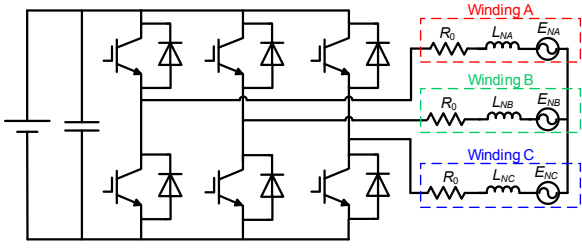
Fig. 2. The drive circuit for the SPM motor in the circuit model.

The mechanical model of the motor can be expressed as

$$\begin{cases} T_e - T_{load} = J_0 \beta \\ w = \int_{t_0}^{t_1} \beta dt \\ \theta = \int_{t_0}^{t_1} w dt \end{cases} \quad (16)$$

where T_{load} is the load torque, β is the angular acceleration, and ω is the angular velocity.

C. Solving Process

Fig. 3 shows the details of the solving process of the dynamic hybrid field model. Two iterative loops are required to solve the DHFM, of which the inner loop calculates the magnetic field distribution of the SPM motor accounting for saturation while the outer loop calculates the phase current based on the circuit and mechanical model at different rotor position.
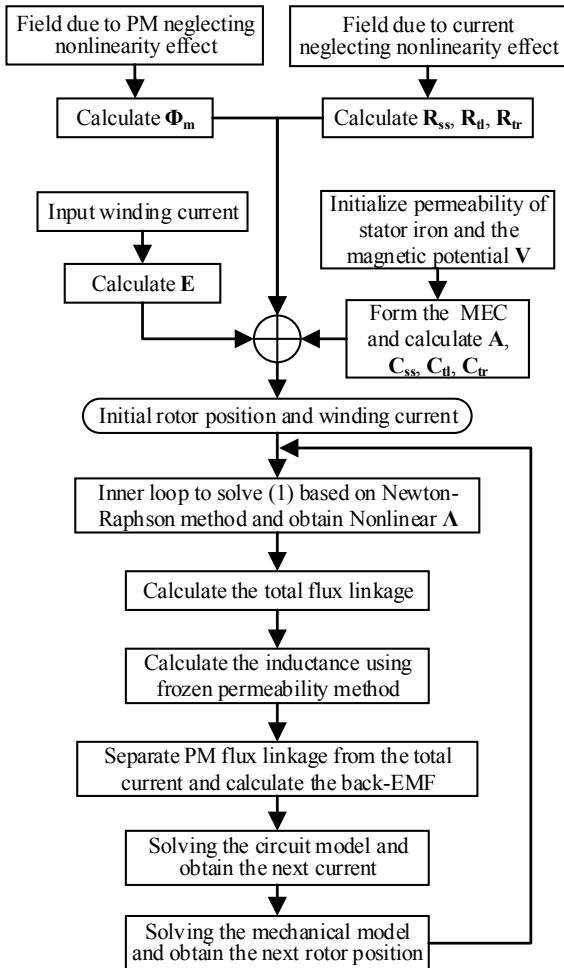
Fig. 3. The general flowchart of solving the DHFM.

III. FINITE ELEMENT VALIDATION

This paper has designed and investigated a 4-pole/15-slot brushless direct current (BLDC) motor running under starting condition to verify DHFM, as shown in Fig. 4. The co-simulation between Ansys Maxwell and Ansys Simplorer is introduced to accurately compute the electromagnetic performance of the BLDC motor under starting condition, as shown in Fig. 5. The static hybrid field model is validated in Fig. 6. It can be seen that hybrid field model exhibits high accuracy as the predicted air-gap field agrees well with FEM results under steady-state condition.
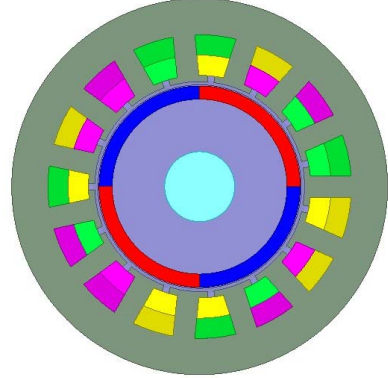

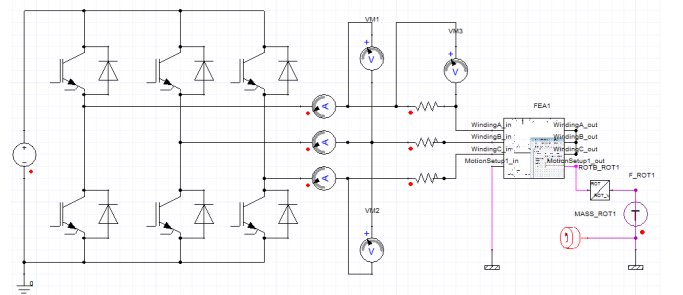Fig. 4. Finite element model of 4-pole/15-slot SPM motor.

Fig. 5. Starting up process of BLDC motor using co-simulation between Ansys Maxwell and Ansys Simplorer.
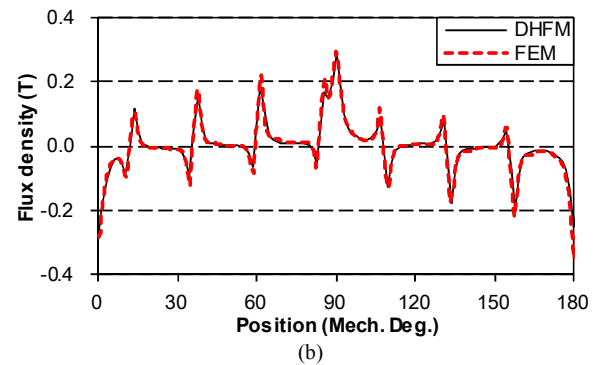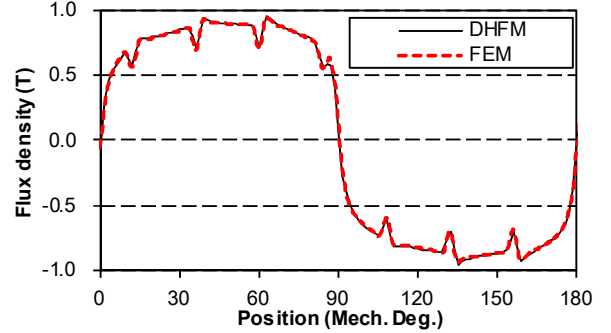

Fig. 6. The flux density at the middle airgap in the SPM motor under steady-state condition: (a) radial and (b) tangential.

In order to show the dynamic performance of SPM motor, the starting condition of the BLDC motor is analyzed. It takes about 630s for DHFM to calculate the electromagnetic performance of the prototype motor while FEM consumes 3869s to obtain the results. The proposed model can save nearly 4/5 computational time of FEM. Figs. 7-8 show that the predicted flux linkage and the induced voltage using DHFM can agree well with the FEM results. Figs. 9 shows that the phase current predicted by DHFM has excellent accuracy. In Fig. 10, the nonlinear inductance using DHFM agrees well with the FEM calculation.
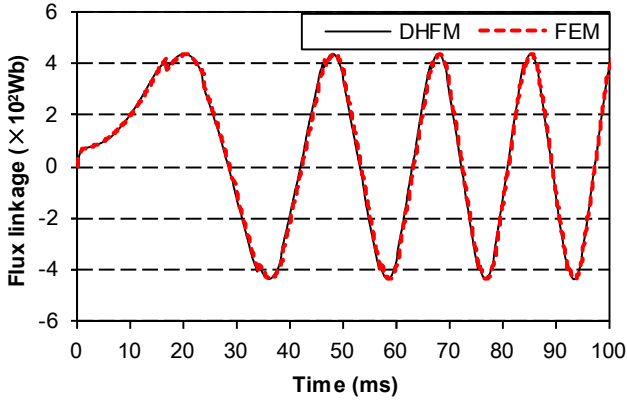
Fig. 7. The flux linkage of Phase A under starting condition.
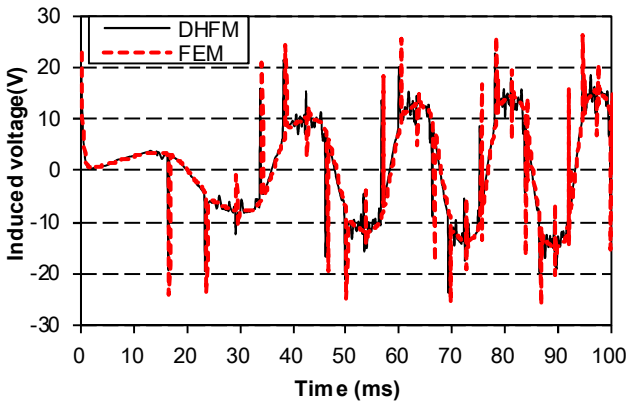
Fig. 8. The induced voltage of Phase A under starting condition.
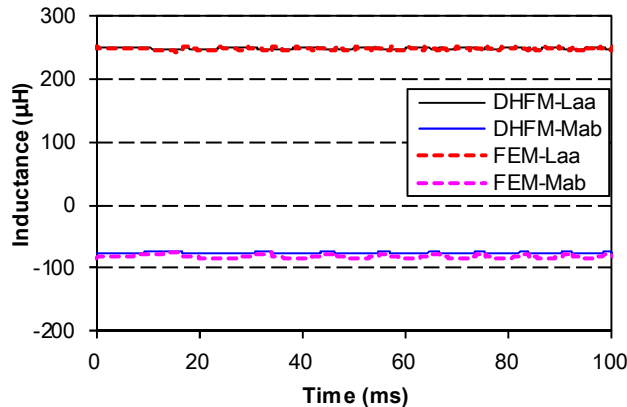

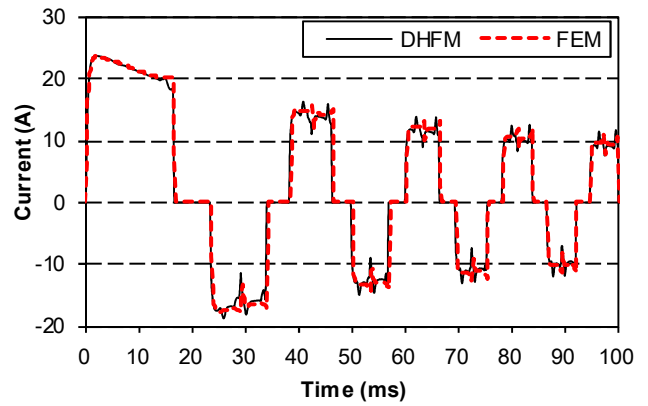Fig. 9. The phase current under starting condition.

Fig. 10. The self and mutual inductance under starting condition.

Fig 11 shows that DHFM can accurately calculate the total torque under starting condition. Besides, DHFM exhibits high accuracy to predict the change of the rotational speed when the SPM motor is started, as shown in Fig 12.
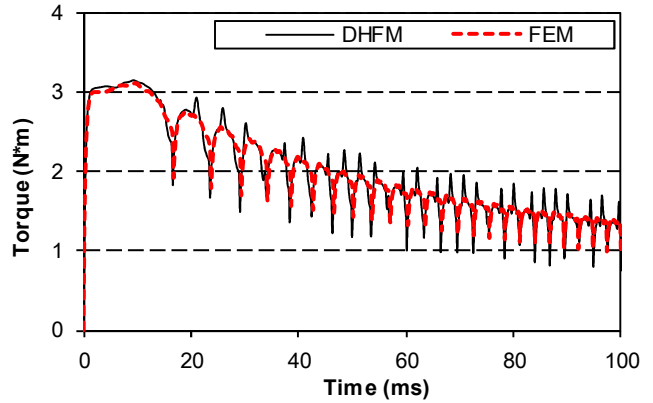

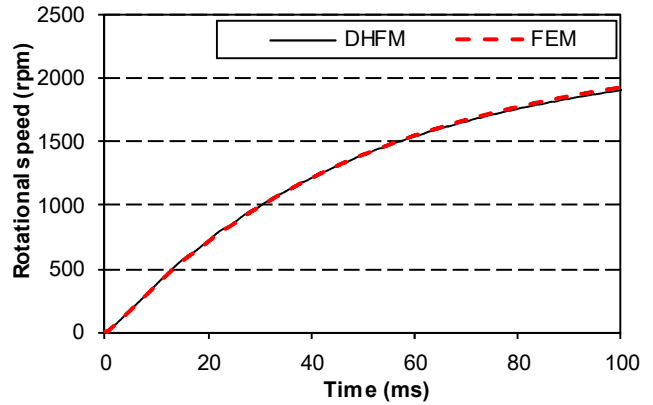Fig. 11. The total torque under starting condition.

Fig. 12. The rotational speed under starting condition.

IV. CONCLUSION

This paper proposed a dynamic hybrid field model to account for the motor saturation in the transient analysis of the SPM motor. The iron saturation can be represented by the analytical expression and therefore the inductance and back-EMF is obtained to analytically replace the SPM motor in the drive circuit. In order to solve the DHFM, two iterative loops are required to consider the saturation effect and show the dynamic performance of the motor. It is demonstrated that the DHFM has great accuracy in predicting the performance of

SPM-type BLDC motor under starting condition while saving 83.7% of computational time using FEM.

REFERENCES

[1] O. A. Mohammed, S. Liu, and Z. Liu, "A phase variable model of brushless dc motors based on finite element analysis and its coupling with external circuits," *IEEE Trans. Magn.,* vol. 41, no. 5, pp. 1576-1579, May 2005.

[2] M. Fazil and K. R. Rajagopal, "Nonlinear dynamic modeling of a single-phase permanent-magnet brushless DC motor using 2-D static finite-element results," *IEEE Trans. Magn.,* vol. 47, no. 4, pp. 781-786, April 2011.

[3] H. Vu Xuan, H. Polinder, D. Lahaye, and J. A. Ferreira, "Modeling for the design of fractional slot PM machines with concentrated windings protected from demagnetization during three-phase short circuit," in *2012 IEEE Energy Conversion Congress and Exposition,* 2012, pp. 1276-1283.

[4] L. J. Wu, Z. Li, X. Huang, Y. Zhong, Y. Fang, and Z. Q. Zhu, "A hybrid field model for open-circuit field prediction in surface-mounted PM machines considering saturation," *IEEE Trans. Magn.,* vol. 54, no. 6, pp. 1-12, June 2018.

[5] L. J. Wu, Z. Li, Dong Wang, Hao Yin, X. Huang, and Z. Q. Zhu, " On-load field prediction of surface-mounted PM machines considering nonlinearity based on hybrid field model" *IEEE Trans. Magn.,* in press.